Appl. Phys. A 81, 963–968 (2005)
DOI: 10.1007/s00339-004-3102-3

Applied Physics A
Materials Science & Processing

C. ARUTA*
F. LICCI✉
A. ZAPPETTINI
F. BOLZONI
F. RASTELLI
P. FERRO
T. BESAGNI

Growth and optical, magnetic and transport properties of $(C_4H_9NH_3)_2MCl_4$ organic-inorganic hybrid films (M = Cu, Sn)

IMEM-CNR, Parco Area delle Scienze 37/A, 43010 Parma-Fontanini, Italy

Received: 7 June 2004/Accepted: 19 October 2004
Published online: 25 November 2004 •

ABSTRACT Films of $(C_4H_9NH_3)_2MCl_4$ (M = Cu and Sn) organic-inorganic hybrid perovskites have been deposited in-situ by a single-source thermal ablation technique on glassy, crystalline and polymeric substrates. Independently of the substrate, the films were well crystallized, c-axis oriented and with a narrow rocking curve of the (0010) reflection (full width at half maximum $< 1°$). The (0 0 ℓ) reflections were consistent with those of the bulk orthorhombic phases and the "c" lattice parameters were 30.85 ± 0.05 and 32.35 ± 0.05 Å, for the Cu- and the Sn-compound, respectively. $(C_4H_9NH_3)_2CuCl_4$ films had an optical absorption peak at 375 nm at room temperature. From the magnetic point of view they act as layered nanocomposites with a dominant ferromagnetic component localized in planes (2D magnetism). T_c was 7.3 ± 0.1 K and a moderate easy-plane anisotropy was observed. The photoluminescence spectra of typical $(C_4H_9NH_3)_2SnCl_4$ films at 12 K had a broad yellow band, which did not correspond to any significant peak in the absorption spectrum. The films were semiconducting down to 250 K or, in the case of the best samples, down to 200 K and became insulating at lower temperature. The resistivity of the best films was $(5 \pm 1)\ 10^4\ \Omega$ cm at 300 K, and the energy gap was 1.11 eV.

PACS 81.07.Pr; 81.15.Kk; 81.16.Dn

1 Introduction

The organic-inorganic hybrid materials provide useful characteristics by coupling the organic and inorganic components at the molecular level. By modulating the electronic structure of the hybrid compounds at the nanometric length scale, it is possible to induce novel electronic and optical properties which do not belong to the organic and inorganic building blocks. In particular, the $(R{-}NH_3)_2MX_4$ and $(NH_3{-}R{-}NH_3)MX_4$ series, consisting of metal halide (MX_4^{2-}) perovskite layers alternated with monoammonium or diammonium cations, are attractive for the potential applications and for the physics understanding [1, 2]. In order to accomplish the charge balancing requirements, the M cation in the inorganic layers is generally a divalent metal which adopts an octahedral coordination. The extended 2D MX_4^{2-} anions are sheeted on both sides by the organic cations, with the ammonium heads hydrogen-ionic bonding to the halogens in the organic sheets. The organic R-group commonly consists of an alkyl chain or a single ring aromatic group. These simple organic layers control the degree of interaction between and the properties arising in the inorganic layers [3]. One of the most interesting features of the hybrid perovskites is the analogy to the multilayer quantum well structures prepared by artificial techniques, such as molecular beam epitaxy. The single-phase, self-assembled hybrids share many interesting properties with the artificial structures, but have the advantage of being intrinsically free of the interfacial roughness between the well and the barrier layers. Moreover, the hybrid-based quantum well structures are quite flexible. The well thickness, well separation, and well depth can be controlled by simply modifying the composition or the stoichiometry of the organic and inorganic components. The quantum well structures give rise to interesting optical phenomena related to the large exciton binding energy, which depends on the metal or halogen atoms in the inorganic component. It has been demonstrated that the organic-inorganic hybrid systems containing germanium(II), tin(II), and lead(II) halides can be efficiently used in light emitting devices by exploiting the possibility of combining the efficient fluorescence of the organic molecules with the tunable electronic band structure of the metal halide sheets [4, 5].

Electronic devices based on organic-inorganic perovskites have also been demonstrated. The high electrical mobility of the inorganic component allows to obtain field effect transistors with mobilities comparable to that of amorphous silicon [6], which represents a significant improvement respect to the purely organic devices. Interesting semiconducting-metal transitions were also observed in tin(II) iodide-based hybrids when increasing the perovskite layer thickness [7, 8].

Moreover, the hybrids containing magnetic cations are ideal models for studying the low-dimensional magnetism phenomena [9]. In particular the paramagnetic cations like Cu(II), which can undergo Jahn–Teller elongation of the octahedral coordination, produce highly flexible systems, with tunable magnetic coupling within the layers and wide variety of magnetic transitions [10].

✉ Fax: +39-0521-269206, E-mail: licci@imem.cnr.it
Permanent address: INFM-Coherentia, Dipartimento di Ingeneria Meccania, Università "Tor Vergata", 00133 Roma, Italy

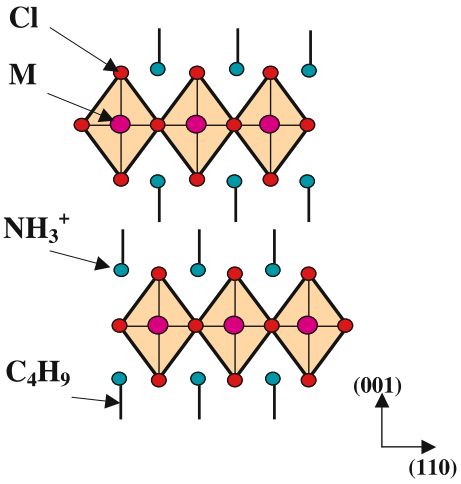

FIGURE 1 Schematic representation of the $(C_4H_9NH_3)_2MCl_4$ structure where M is Cu^{2+} or Sn^{2+}

Finally, the availability of perovskite hybrids in form of oriented films is fundamental for technological applications. In particular, thin layers are essential for producing heterostructures to be used in integrated electronics. The organic-inorganic films have been grown by different solution-based or evaporative growth techniques [6, 11–13]. The solution-based deposition methods (such as spin-coating, ink-jet printing, stamping and spray coating) require the use of the proper solvents, which enable the efficient hybrid solubility and substrate wetting. These requirements are not easily achieved and the evaporative techniques in a few cases are more convenient. In particular, the single-source thermal ablation (SSTA) technique has demonstrated to be a successful and versatile method for the in situ deposition of $(R{-}NH_3)_2MX_4$ hybrid films, with SnI_4^{2-} and PbX_4^{2-} (X = Br and I) perovskite layers and suitable structural and physical properties [14, 15]. By using the SSTA method, we have grown for the first time $(C_4H_9NH_3)_2MCl_4$ films with M = Cu(II) and Sn(II). The basic structure of the compounds is schematically depicted in Fig. 1. Copper(II) and tin(II) chloride ⟨100⟩ perovskite sheets are shifted between adjacent layers ("staggered" arrangement) and the organic tails extend into the space between the perovskite sheets. Van der Waals interaction between the tails of the organic component hold the perovskite layers together in the structure. In this report we describe the deposition procedure and several structural and physical properties of the hybrid films.

2 Experimental

2.1 *Precursors and film deposition*

$(C_4H_9NH_3)_2MCl_4$ films with M = Cu and Sn were grown in situ by the SSTA technique. The ablation of the film precursors was carried out in a home-made apparatus, similar to that described by Mitzi et coworkers [11, 15]. A 0.1–0.2 mm thin tantalum foil was used as crucible.

The $(C_4H_9NH_3)_2CuCl_4$ precursor was a single-phase homogeneous compound with the same composition of the film. It was obtained by dissolving in ethanol the stoichiometric amount of $CuCl_2 \cdot 2H_2O$ (Merck 99%) and of $C_4H_9NH_3Cl$ (home-prepared [16]) and by evaporating the solvent [1]. As an example, for producing about 1 g of $(C_4H_9NH_3)_2CuCl_4$, 0.44 g of $CuCl_2 \cdot 2H_2O$ and 0.56 g of $C_4H_9NH_3Cl$ were dissolved in 10–20 ml of ethanol. The solution was evaporated until a gold-yellow precipitate formed. The precipitate was filtered, washed several times with a few ml of ethanol and finally with ether, and dried in air, at ≈ 40 °C. When examined by X-ray powder diffraction it resulted to be orthorhombic, single-phase $(C_4H_9NH_3)_2CuCl_4$ [17]. About 0.1 g of the precipitate were dispersed in 0.5 ml ethanol by sonicating for 15 min. Several drops of the suspension were taken off and placed on the crucible within the vacuum chamber.

$(C_4H_9NH_3)_2SnCl_4$ films were obtained from precursors consisting of ethanol solution of stoichiometric amounts of $C_4H_9NH_3Cl$ and $SnCl_2$ (Fluka 98%). Typically, 0.05 g of $C_4H_9NH_3Cl$ and 0.0425 g of $SnCl_2$ were dissolved in 0.25 ml of ethanol by sonicating for 15 min. 10 drops of the resulting solution were transferred into the crucible for the ablation.

Different materials were used as substrates, including glass, quartz, Mylar polyester, polystyrene, alumina, and $SrTO_3$, MgO or Si crystals. They were approximately 5 × 5 or 10 × 10 mm^2, placed face down, "on axis" at 8 cm from the heater, and held at room temperature.

The ultimate system pressure just before the thermal ablation was in the low 10^{-5} mbar. A large current (≥ 150 A) was passed through the tantalum foil, thus enabling the thermal ablation of the precursor from the foil toward the substrate.

The deposition process accomplished for few seconds (< 5 s) and an almost instantaneous ablation occurred.

After depositing, we maintained the films in a dry-box, under argon atmosphere.

2.2 *Characterization*

The film thickness was measured a-posteriori by a standard profilometer and roughly calibrated by varying the amount of the precursor (i.e., the drop number) placed on the crucible.

The precursor and the film crystal structure and the "c" lattice parameter were determined by X-ray diffraction, taken on a D-500 Siemens diffractometer, with a Cu K_α radiation.

The optical absorption was measured at room temperature, by a JASCO V-530 spectrophotometer. The photoluminescence was induced by a He-Cd laser with an excitation wavelength = 326 nm. The relevant spectra were collected at 12 K.

The magnetic susceptibility vs. temperature was measured in the 4.2–300 K range, and the experimental data were corrected for the demagnetizing factor. The measurements were done in a commercial radio-frequency SQUID magnetometer. The magnetic field was applied in two orthogonal directions, either perpendicular or parallel to the film surface, that means, to a large extent, parallel to the *c*-axis or parallel to the a-b plane, respectively.

The electrical transport characteristics were determined by applying 10 V through the sample, and by detecting the current with a pico-ammeter in a four-contact geometry. The substrate was partially covered by the film and the electrical contacts were obtained by evaporating on the top of the film four thin Ag stripes, terminating with large pads directly on the substrate. The pads were taken far from the film in order to

avoid the degradation during the soldering of the copper wires with indium. The absolute value of the resistivity was determined by using a commercial linear four-probe head with the tip spacing = 0.65 mm.

3 Results and discussion

Under the described conditions the organic and inorganic components simultaneously evaporate from the heater, in spite of the significant differences in the physicochemical and thermal properties. In particular, the very fast ablation kinetics preserves the organic component from any significant decomposition.

The choice of the appropriate precursor was done on the basis of the chemical characteristics of the reagents. The homogeneous precursor was preferred in the case that both, the metal and the ammine halides, were stable and soluble in a common solvent from which the hybrid precipitated. Such conditions occurred in the case of the Cu system. On the contrary, the hybrid Sn-compound was highly soluble in ethanol, and only yielded a gelatinous residual after completely evaporating the liquid. As a consequence, the complex Sn(II)/Sn(IV) redox equilibrium and the precipitate stoichiometry were hardly controllable. In this case the stoichiometric reagent solution was more reliable as the film precursor.

The quality of the films came out quite insensitive to the base pressure in the range 5×10^{-5}–5×10^{-6} mbar but fairly sensitive to the current through the tantalum foil. The appropriate amount of the current had to be optimized by trial, and periodically adjusted as a function of the crucible ageing and geometry and of the specific precursor.

The structure and morphology of the film were independent of the type and the texture of the substrate.

The typical thickness of the films was 100–500 nm when ablating for 20 s about 100 mg of precursor. Optical microscopy pictures showed the presence of precipitates on the surface, which are typical of the ablation processes. The film surface roughness was of the order of 10 nm.

3.1 $(C_4H_9NH_3)_2CuCl_4$ films

The bulk Cu(II)-halide hybrid perovskites have been widely investigated for the interest in the Jahn–Teller distorsions and the magnetic interactions [10]. Conversely, to our knowledge, data on the hybrid films have not yet been reported.

The X-ray θ–2θ diffraction pattern shown in Fig. 2 corresponds to an optimized 500 nm thick and 5×5 mm large $(C_4H_9NH_3)_2CuCl_4$ film, grown on a glass substrate. It indicates that the film is single-phase and highly-oriented with the plane of the perovskite layer parallel to the surface of the substrate (c-axis growth). Only the (0 0 ℓ) reflections are in fact visible. In addition, the existence of the high order reflections (until $\ell = 16$) indicates that the film is well crystallized. The rocking curve, measured along the (0010) reflection (inset of Fig. 2) gave a full width at half maximum $< 1°$. The calculated c-axis parameter of the cell is $= 30.85 \pm 0.05$ Å, slightly larger than that measured in the orthorhombic bulk samples (30.75 Å) ([17] and this work).

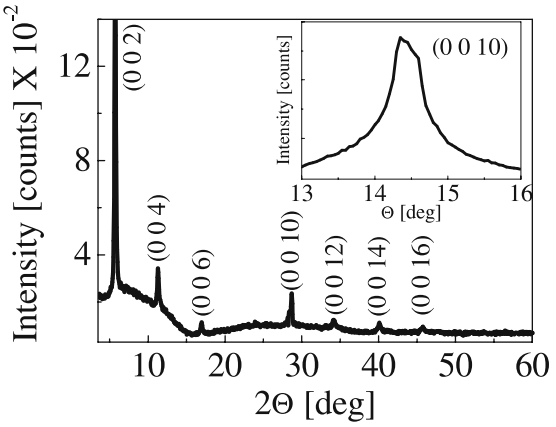

FIGURE 2 Typical X-ray diffraction spectrum of glass-deposited $(C_4H_9NH_3)_2CuCl_4$ films. The approximate film thickness and the surface area were 500 nm and 5×5 mm, respectively. The rocking curve of the (0010) reflection is shown in the *inset*

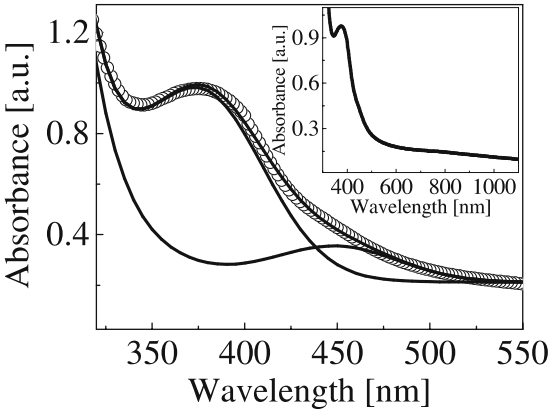

FIGURE 3 Optical absorbance of a glass-deposited $(C_4H_9NH_3)_2CuCl_4$ film vs. wavelength at room temperature. The *lines* are the fit to the sum of two Gaussians with the exponential background of the substrate. *Inset*: absorbance in the 300–1100 nm wavelength range

The optical absorbance measurements reported in Fig. 3 were reproducibly obtained at room temperature from the $(C_4H_9NH_3)_2CuCl_4$ films deposited on glass substrates. They show the first $Cl^- - Cu^{2+}$ charge transfer π–d transition, due to the D_{4h} symmetry, around 375 nm [18, 19]. The spectrum of Fig. 3 has been fitted to the sum of two Gaussian (full lines) enlightening the presence of a second weaker transition at lower energy. It may likely be associated to the actual D_{2h} symmetry of the $CuCl_6^{4-}$ complex, as reported for the $(C_3H_7NH_3)_2CuCl_4$ compound [19]. In the inset of Fig. 3 the 300–1100 nm range of the optical spectrum is shown. A broad absorption band centered at about 800 nm is evident. It was already observed in presence of Cu with the square planar coordination [17] and attributed to the crystal field d–d transitions.

Because of the antiferrodistorsive arrangement of the Cu–Cl bonds within the $CuCl_4^{2-}$ sheets, the magnetic orbitals on adjacent Cu(II) ions are nearly orthogonal (the overlap integral is essentially zero), thus leading to a ferromagnetic exchange [9], differently from the predominantly antiferromagnetic interactions occurring within the perovskite sheets in the non-Jahn–Teller compounds (such as $(C_4H_9NH_3)_2MCl_4$ with M = Mn(II) or Fe(II) [3]. $(C_4H_9NH_3)_2CuCl_4$ has proved to be quasi two-dimensional due not only to the layered structure,

but also to the fact that adjacent layers are staggered such that dipolar interactions between nearest neighbor layers are substantially reduced. However, in addition to the strong in-plane ferromagnetic interaction, a weak antiferromagnetic coupling between the layers is present [9]. The magnetic susceptibility of the quartz-deposited films vs. temperature is shown in Fig. 4a. The Curie temperature, T_c, was determined from the maximum in the derivative of the magnetization vs. temperature. The obtained value was 7.3 ± 0.1 K for both, the powder precursor and the film. For the latter, T_c was independent of the direction of the magnetic field, either parallel or perpendicular to the c-axis. Such a T_c value is consistent with the literature data [3]. In Fig. 4b the inverse molar susceptibility of the powder precursor and of the film are reported together with the fit to the Curie–Weiss law at $T > T_c$, $\chi^{-1} = (T - \Theta)/C$ (where Θ and C are the Weiss and the Curie constants, respectively). The intercept of the fitted data at $T > 0$ confirms that the dominant interaction is ferromagnetic. The low magnetic moment of the paramagnetic phase, at the limit of the SQUID sensitivity, hindered to extend the relatively narrow range of the measurement temperature relevant to the film. At low temperature the upward curvature of the $1/\chi$ plot suggests that the Curie–Weiss law is not more valid. Such a behavior is characteristic of the short-range interactions or low dimensional order. Accordingly, the T_c value resulting from the linear extrapolation of $1/\chi$ is higher than the effective one.

The intercept and the slope of the Curie–Weiss fit represent the Weiss constant, Θ, and the Curie constant, C, respectively, with $C = N\mu_B^2 p^2/3kT$, and $p^2 = g^2 S(S+1)$. From the fit we get $\Theta = (18.3 \pm 0.3)$ K and $p = (1.9 \pm 0.5)\,\mu_B$, in reasonable agreement with the value of the Cu(II) magnetic moment calculated on the basis of the Hund rule ($1.73\,\mu_B$) [20]. The difference between the susceptibility values measured in the direction parallel to the c-axis of the film and perpendicularly to it (Fig. 4a) suggests that the compound is anisotropic and that the c-axis represents the hard direction. The available data, however, do not allow one to accurately determine the strength of the anisotropy field, because they were collected under a too low magnetic field. The ratio between the susceptibility measured along the c-axis and perpendicularly to it, which is proportional to the anisotropy, was estimated to be ≈ 0.5, lower than the corresponding value measured in single crystals of $[C_6H_5(CH_2)_nNH_3]_2CuCl_4$ related compounds [21]. The discrepancy may be imputed to the compositional difference between the films and the literature crystals. In addition, in the case of the film, the in-plane structural disorder cannot be ruled out. The organic cations, from one side, easily rotate around the C–N group, thus influencing the local atomic distribution of the inorganic components but not the overall crystal structure. From the other side, the grains of the film, grown on a non-oriented, polycrystalline quartz substrate, are expected to be randomly distributed in the "ab" plane. Such features have to be taken into account when evaluating the anisotropy from the magnetic susceptibility data.

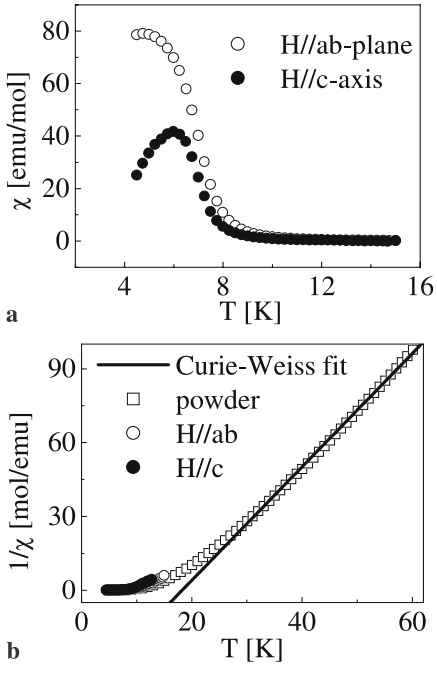

FIGURE 4 (**a**) Magnetic susceptibility of a quartz-deposited $(C_4H_9NH_3)_2CuCl_4$ film vs. temperature. The magnetic field was 10 Oe, applied parallel to either, the a-b plane and the c-axis. (**b**) Inverse molar susceptibility vs. temperature of the powder precursor and of the film, measured with the two field directions. Straight line indicates the Curie–Weiss fit at $T > T_c$. All the experimental data were corrected for the demagnetization factors

3.2 $(C_4H_9NH_3)_2SnCl_4$ films

The crystallographic quality of $(C_4H_9NH_3)_2SnCl_4$ is similar to that of $(C_4H_9NH_3)_2CuCl_4$ films. Sn(II) is relatively stable against oxidation when incorporated in the film. Moderate variations of the diffraction pattern, imputable to the presence of Sn(IV), were only detected after several days of air exposure. The X-ray pattern shown in Fig. 5 corresponds to a 500 nm thick and 10×10 mm large film, deposited on a glass substrate. It is highly c-axis oriented and the c parameter is 32.35 ± 0.05 Å. This value is consistent with that measured in the polycrystalline compound having the orthorhombic structure [22].

$(R{-}NH_3)_2MX_4$ hybrids with M = Sn and X = I are reported to have interesting transport properties [6, 7, 23], which are correlated to the structural parameters, mainly the Sn–I average bond length and the SnI_6 octahedron distortion. Namely, as the bond length and the distortion decrease,

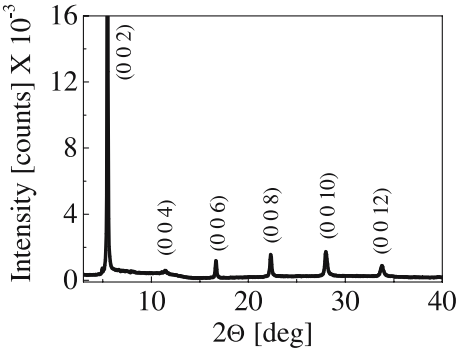

FIGURE 5 X-ray diffraction spectrum of a typical glass-deposited $(C_4H_9NH_3)_2SnCl_4$ film. The approximate film thickness and the surface area were 500 nm and 10x10mm, respectively

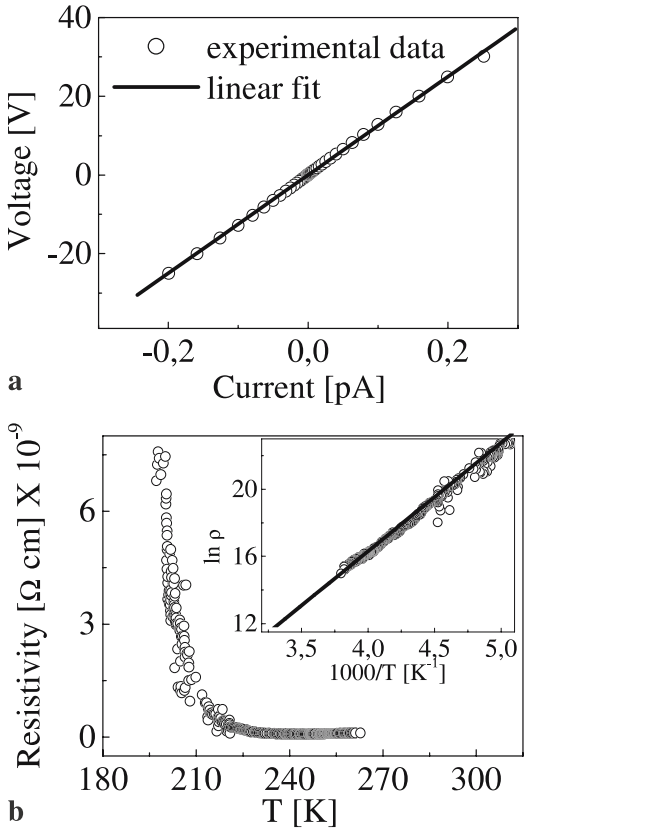

FIGURE 6 Electrical characteristics of glass-deposited $(C_4H_9NH_3)_2SnCl_4$ films: (**a**) *I–V* characteristic and linear fit (*continuous line*); (**b**) resistivity vs. temperature. *Inset*: natural logarithm of resistivity vs. $1/T$ and fit to a Mott insulator behavior (*continuous line*)

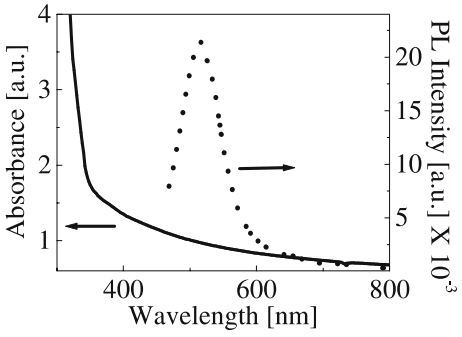

FIGURE 7 Optical absorption spectrum at room temperature (*continuous line*) and photoluminescence spectrum at $T = 12$ K (*dotted line*) of a glass-deposited $(C_4H_9NH_3)_2SnCl_4$ film

the conductivity of the materials increase (i.e., the band gap decreases) [8]. Accordingly to such statements and by assuming that the octahedron distortion remains unchanged, the R−$SnCl_4$ hybrids should be expected to be better conductors than the corresponding R−SnI_4. In Fig. 6 we show the *I–V* characteristic, (Fig. 6a) and the resistivity vs. temperature (Fig. 6b) of a glass-deposited $(C_4H_9NH_3)_2SnCl_4$ film. In the inset of Fig. 6b the natural logarithm of resistivity vs. $1/T$ and the calculated fit to a Mott insulator behavior are shown. Most of the samples resulted insulating at ≈ 250 K, while the resistivity vs. temperature data of the best samples indicated that they are semiconducting down to ≈ 200 K (Fig. 6b). In this respect the chloride films are comparable to the polycrystalline $(C_4H_9NH_3)_2SnI_4$ pressed pellets [7]. As far as the absolute value of the resistivity is concerned, it is affected by the sample roughness and inhomogeneity. By taking into account such factors and the thickness uncertainty, we estimated an error $\approx 20\%$ on the experimental values. The lowest resistivity we measured at room temperature was $5 \times 10^4\ \Omega$ cm, comparable to that of $(C_4H_9NH_3)_2SnI_4$ pressed pellets ($\approx 10^5\ \Omega$ cm) [7].

As for other semiconducting hybrids [8], the temperature dependence of the resistivity is well described by the Mott insulator law, i.e.: $\varrho = A \exp(E_g/2k_BT)$, where A is a constant, E_g the band gap, k_B the Boltzmann's constant and T the temperature. The resistivity of the best films is well fitted by assuming $E_g = 1.11$ eV. Such a value is higher than the corresponding one measured on $[NH_2C(I)=NH_2]_2(CH_3NH_3)_2Sn_2I_8$ pressed pellets (0.33 eV) [8]. The difference is reasonably due to the fact that the reduction of the Sn–X bond length ($Cl^- < I^-$ ionic radius) is compensated by both, the lower dimensionality of the structure (the perovskite layers are thinner in $(C_4H_9NH_3)_2SnCl_4$ than in $[NH_2C(I)=NH_2]_2(CH_3NH_3)_2Sn_2I_8$) and the larger distortion of the $SnCl_6$ octahedra with respect to SnI_6 [3, 7].

The optical properties of $(C_4H_9NH_3)_2SnCl_4$ films were measured on freshly prepared specimens deposited on glass substrates. Figure 7 shows the optical absorption spectrum (continuous line) and the photoluminescence (Pl) spectrum (dotted line). No exciton absorption peaks appear in the absorption spectrum. This is consistent with the previous data relevant to $(C_4H_9NH_3)PbX_4$ films [2], which indicate that the exciton absorption peak shifts from the visible towards the UV region by decreasing the halide atomic weight from iodine to chlorine. Conversely, the Pl spectrum at $T = 12$ K exhibits a broad yellow luminescence band. A similar band was observed in the $(C_6H_{13}NH_3)_2SnCl_4$ and $(C_8H_{17}NH_3)_2SnCl_4$ crystals [22] and attributed to the lowest exciton transition from the bottom of the Sn($5p$) band to the top of the Sn($5s$) band. Such an assumption is not consistent with the fact that the corresponding absorption band is lacking (Fig. 7). In addition, the broad shape of the Pl band is atypical for the exciton emission. In our opinion it seems more reasonable to attribute the luminescence band to the presence of an unidentified defect state. The point however deserves further investigations.

3.3 *Conclusions*

We have demonstrated the feasibility of $(C_4H_9NH_3)_2MCl_4$ (M = Cu, Sn) organic-inorganic hybrid films on crystalline, glassy or plastic substrates by the SSTA technique. The films were grown in-situ, at room temperature, and resulted to be *c*-axis oriented. They exhibited good structural and physical properties, consistent with those of the related bulk compounds. In particular, $(C_4H_9NH_3)_2CuCl_4$ films were 2D magnetic nanocomposites, with a dominant ferromagnetic component localized in planes and the ordering temperature $= 7.3 \pm 0.1$ K. They also showed optical absorption at 375 nm. The best $(C_4H_9NH_3)_2SnCl_4$ films were semiconducting down to 200 K and became insulating at lower temperature. The resistivity was $(5 \pm 1)10^4\ \Omega$ cm at 300 K and the energy gap was 1.11 eV. The relevant photolumines-

cence spectra contained a broad yellow band, which did not correspond to any significant peak in the absorption spectrum.

ACKNOWLEDGEMENTS The authors thank F. Bigi for the fruitful discussions and E. Gombia, A. Cassinese and A. Priggiobbio for the electrical measurements.

REFERENCES

1 H. Arend, W. Huber, F.H. Mischgofsky, G.K. Richter-van Leeuwen: J. Cryst. Growth **43**, 213 (1978)
2 D.B. Mitzi, K. Chondroudis, C.R. Kagan: IBM J. Res. & Dev. **45**, 29 (2001)
3 D.B. Mitzi: Progr. Inorg. Chem. **48**, 1 (1999)
4 X. Hong, T. Ishihara, A.V. Nurmikko: Phys. Rev. B **45**, 6961 (1992)
5 D.B. Mitzi: Chem. Mater. **8**, 791 (1996)
6 C.R. Kagan, D.B. Mitzi, C.D. Dimitrakopoulos: Science **286**, 945 (1999)
7 D.B. Mitzi, C.A. Feild, W.T.A. Harrison, A.M. Guloy: Nature **369**, 467 (1994)
8 D.B. Mitzi, S. Wang, C.A. Feild, C.A. Chess, A.M. Guloy: Science **267**, 1473 (1995)
9 L.J. de Jongh, A.R. Miedema: Adv. Phys. **23**, 1 (1974)
10 R. Willett, H. Place, M. Middleton: J. Am. Chem. Soc. **110**, 8639 (1988)
11 D.B. Mitzi: Chem. Mater. **13**, 3283 (2001)
12 M. Era, T. Hattori, T. Taira, T. Tsutsui: Chem. Mater. **9**, 8 (1997)
13 K. Liang, D.B. Mitzi, M.T. Prikas: Chem. Mater. **10**, 403 (1998)
14 K. Chondroudis, D.B. Mitzi, P. Brock, P. Brock: Chem. Mater. **12**, 169 (2000)
15 D.B. Mitzi, M.T. Prikas, K. Chondroudis: Chem. Mater. **11**, 542 (1999)
16 See, e.g., J. Zabicky: In *The Chemistry of the Amino Group*, ed. by S. Patai (Wiley, New York 1968) Chapt. 3, p. 79
17 D. Abdelaziz, A. Thrierr-Sorel, R. Perret, B. Chaillot, J.E. Guerchais: Bull. Soc. Chim. France **103**, 535 (1975)
18 Y. Morimoto, Y. Tokura: J. Chem. Phys. **101**, 1763 (1994)
19 R. Valiente, F. Rodríguez: Phys. Rev. B **60**, 9423 (1999)
20 A.H. Morrish: *The Physical Principles of Magnetism* (Wiley, New York 1965)
21 W.E. Estes, D.B. Losee, W.E. Hatfield: J. Chem. Phys. **72**, 630 (1980)
22 Ri-Zhu Yin, Chul Hyun Yo: Bull. Korean Chem. Soc. **19**, 947 (1998)
23 D.B. Mitzi, C.A. Feild, Z. Schlesinger, R.B. Laibowitz: J. Solid State Chem. **114**, 159 (1995)